Growth evolution of laser-ablated Sr_2FeMoO_6 nanostructured films: Effects of substrate-induced strain on the surface morphology and film quality

H. Jalili,[1,a)] N. F. Heinig,[2] and K. T. Leung[1,2,b)]
[1]*Department of Physics and WATLab, University of Waterloo, Waterloo, Ontario N2L 3G1 Canada*
[2]*Department of Chemistry and WATLab, University of Waterloo, Waterloo, Ontario N2L 3G1 Canada*

(Received 12 February 2010; accepted 30 March 2010; published online 25 May 2010)

Pulsed laser deposition was used to grow Sr_2FeMoO_6 films of different thicknesses on MgO(100), $SrTiO_3$(100), and $LaAlO_3$(100) with respective lattice mismatches of +6.2%, −1.2%, and −4.3%. Surface roughness and morphology, and film crystal quality and epitaxy were determined by atomic force microscopy and x-ray diffraction, respectively. Two-dimensional layer-by-layer growth was evident for the Sr_2FeMoO_6 grown on MgO and $SrTiO_3$ with the film becoming smoother with increasing thickness. The Sr_2FeMoO_6 films had more nucleation sites on MgO than $SrTiO_3$. On $LaAlO_3$, however, three-dimensional progressive growth of flakelike Sr_2FeMoO_6 nanostructures was observed for all film thicknesses. High-resolution x-ray diffraction measurements indicated that the Sr_2FeMoO_6 films are near-epitaxial and c-axis oriented on all the substrates. Reciprocal space maps further revealed that Sr_2FeMoO_6 grows on MgO with relatively constant lattice parameters with increasing film thickness. For films thicker than 120 nm, the formation of a second phase was observed on $SrTiO_3$ and $LaAlO_3$ but not on MgO, suggesting that the formation of a second phase provides an effective strain relief in the former. These results suggested a different growth mechanism for the Sr_2FeMoO_6 films on MgO compared to the $SrTiO_3$ and $LaAlO_3$ substrates.
 [doi:10.1063/1.3407453]

I. INTRODUCTION

Double perovskite Sr_2FeMoO_6 (SFMO) has long been known as a conducting ferromagnet (or ferrimagnet) with a relatively high Curie temperature of 410–450 K.[1] Kobayashi *et al.* reported a low-field magnetoresistant response for this double perovskite material at room temperature, and their companion electronic calculations suggested a half-metallic nature.[2] The high degree of spin polarization in this material was later confirmed by Bibes *et al.*[3] These studies identified SFMO as a potential candidate for spin-based electronic (spintronic) devices at room temperature. The magnetic and electronic properties of SFMO are highly dependent on the crystal quality, grain size, and the presence of defects (including antisite defects and grain boundaries).[4,5] In magnetic oxide films (e.g., $SrRuO_3$ and $La_xSr_{1-x}MnO_3$), it is possible to control the formation of domains and secondary phases by manipulating the lattice parameters with different growth conditions (such as temperature and deposition time), hydrostatic pressure, or use of substrates with a different crystal lattice mismatch to the films.[6–10] In order to exploit the half-metallic character of SFMO and to prevent spin scattering at the surface/interface in the spintronic devices, it will be necessary to produce high quality films with a sharp surface/interface. In the present work, we investigate the effects of substrate-film lattice mismatch and film thickness on the crystallographic properties of the as-grown SFMO films, with the goal to provide better understanding about the film growth process appropriate for spintronic devices.

SFMO films have been grown by pulsed laser deposition (PLD)[11–17] and magnetron sputtering[18,19] at various deposition temperatures between 320 and 950 °C. The properties of interest are usually the magnetic moment, resistivity, and Curie temperature. Films grown at a low deposition temperature tend to be semiconducting with a low magnetic moment, which has been attributed to Fe/Mo site disorder.[14,15] At a higher growth temperature, site disorder is expected to be reduced, which would increase the magnetization. However, the magnetization could also be increased due to the presence of the so-called parasitic phases, including Fe-rich secondary phases,[11,12,16] which form at a high growth temperature. In addition to the growth temperature, the choice of the substrate is also important. The most common substrate for growing SFMO films has been $SrTiO_3$(100) (or STO) due to their good lattice matching (with a −1.2% lattice mismatch).[11–15] SFMO films have also been grown on several other substrates, including STO(111), MgO(100) (with a +6.2% lattice mismatch), and $LaAlO_3$(100) (or LAO, with a −4.3% lattice mismatch), as well as polycrystalline $Sr_{0.5}Bi_{0.5}TiO_3$.[16–19] Significant discrepancies in the properties of films grown on different substrates have been found. In particular, several groups[16,18,19] have examined the influence of strain induced by lattice mismatch on SFMO. Borges *et al.*[16] used PLD to grow epitaxial SFMO on STO(100) and MgO(100) and compared their transport and magnetic properties. They concluded that the number of defects found in

[a)]Present address: Massachusetts Institute of Technology, Cambridge, MA 02139, USA.
[b)]Author to whom correspondence should be addressed. Electronic mail: tong@uwaterloo.ca.

the SFMO film grown on MgO was sensitive to the deposition temperature and the films grown on STO exhibit better physical properties than those grown on MgO. Asano *et al.*[19] used magnetron sputtering to epitaxially grow SFMO on STO(100) and MgO(100) and found differences in their magnetic and magneto-optical properties, which they attributed to antisite disorder on the Fe and Mo sites caused by substrate-induced lattice strain/relaxation. Boucher[18] also used magnetron sputtering to grow SFMO on STO(100), MgO(100), LAO(100), and polycrystalline $Sr_{0.5}Bi_{0.5}TiO_3$ and studied the effect of film thickness and substrate-induced strain on the films. His results showed that the best crystal structure was obtained on the STO substrate, while elemental compositional changes were found in films grown on MgO and LAO with different thicknesses.

The aforementioned studies have shown that high quality SFMO films can be obtained by PLD. In the present work, we use PLD to deposit SFMO films with different thicknesses on STO(100), MgO(100), and LAO(100) in order to provide a systematic study of the strain induced by substrate-film lattice mismatch and their effects on growth evolution. Optimized growth conditions have been used to obtain epitaxial single-phase SFMO films on MgO (Ref. 20) and the other substrates. In our earlier work,[20] we studied the growth conditions of PLD-grown SFMO films on MgO and characterized the films by x-ray photoemission and magnetization measurements. The saturation magnetic moment of the SFMO film on MgO was measured at 5 K with the magnetic field parallel to the film surface and was found to be 3.4 ± 0.1 μ_B/f.u. The good agreement of the measured moment to the theoretical value (4.0 μ_B/f.u.) was indicative of a high quality film. In the present work, in order to minimize variations in the growth conditions, we deposit the SFMO films simultaneously on all three substrates (MgO, STO, and LAO). Their surface roughness and morphology are determined by atomic force microscopy (AFM), while the lattice parameters and crystal quality are characterized by high-resolution x-ray diffraction (XRD) using ω-2θ scans and reciprocal space mapping (RSM).

II. EXPERIMENTAL DETAILS

A NanoPLD system (PVD Products, Wilmington, MA) equipped with a KrF excimer laser (with a maximum laser fluence of 600 mJ/pulse) was used for the film growth experiments in a base vacuum better than 5×10^{-7} Torr. Epi-polished MgO(100), STO(100), and LAO(100) were purchased from MTI Corp. and used in as-received form as substrates for growing the epitaxial films. The 1 in. diameter SFMO target (99.95% purity) was also obtained commercially (from MTI). With the substrates held at a fixed temperature of 800 °C and a target-to-substrate distance set to 42 mm, films were deposited on all three substrates simultaneously for a preselected period of time (5, 10, 30, 40, and 50 min). The laser was operating at a repetition rate of 10 Hz and a laser fluence of 400 mJ/pulse, delivering a power density of $4-5$ J/cm^2 to the target.

For each growth condition, the morphology of the resulting film was characterized by using a DI Nanoscope IV, AFM operated in tapping mode. To characterize the strain and crystalline quality of the film, high-resolution Bragg diffraction and RSM were carried out using a Panalytical X-Pert Pro MRD x-ray diffractometer, with the Cu K_α source operated at 45 kV tension and 40 mA current. For the Bragg XRD studies, a Ge(220) two-bounce hybrid monochromator with a 1/2° slit and a triple-axis section with a 1/16° slit were used to define the incident and diffracted beams, respectively. For the RSM measurements, the 1/16° slit was replaced by a channel-cut Ge(220) analyzer in the triple-axis section for the diffracted beam optics (without changing the incident beam optics).

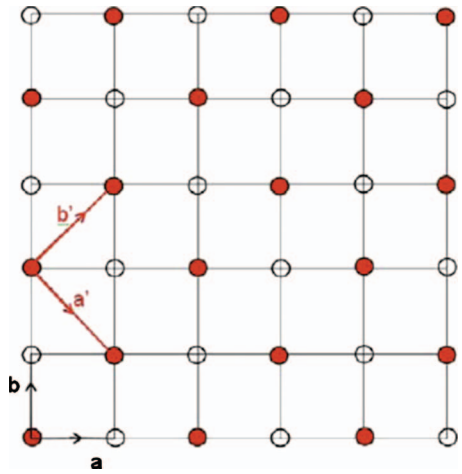

FIG. 1. Two-dimensional schematic diagram of the cubic lattice structure of the substrate (open circles) with a and b lattice vectors and the (110) plane of Sr_2FeMoO_6 (solid circles) with a′ and b′ lattice vectors. The c axes are out of plane.

III. RESULTS AND DISCUSSION

To minimize the strain induced by the STO(100), LAO(100), and MgO(100) substrates, SFMO will grow along its c-axis in parallel to the c axes of the substrates,[11,15,18,19] with the a and b axes of SFMO lying in the [110] and [1$\bar{1}$0] directions, respectively, of the substrates. Figure 1 shows a schematic diagram depicting the crystallographic relation of the SFMO film with respect to the substrate lattice. The lattice mismatch between SFMO [a=b =5.5870 Å and c=7.9180 Å (Ref. 21)] and the cubic substrates of MgO [a=b=c= 4.2112 Å (Ref. 22)], STO [a=b =c=3.9050 Å (Ref. 23)], and LAO [a=b=c=3.7890 Å (Ref. 24)] can be calculated by using the following expression: $[x_{substrate} - (\sqrt{2}/2)x_{SFMO}]/x_{substrate}$, where $x_{substrate}$ and x_{SFMO} are the (a, b) lattice parameters of the substrate and SFMO, respectively. The lattice mismatch values obtained for MgO, STO, and LAO are +6.2%, −1.2%, and −4.3%, respectively. An alternative epitaxial relationship with SFMO on STO has been observed by Borges *et al.*,[16] where the (surface normal) c axis of the substrate is parallel to the SFMO(220) direction and the SFMO c-axis lies along the STO (a,b) surface. This type of orientation also gives a low mismatch strain but was not observed in our films. While it is difficult to distinguish the (004) and (220) peaks from the Bragg (ω-2θ) scan alone, we confirmed the identification of

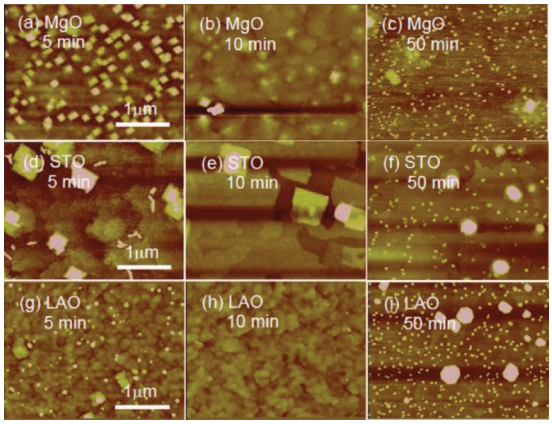

FIG. 2. AFM images of Sr_2FeMoO_6 films grown for selected deposition times of 5 min (left column), 10 min (center column), and 50 min (right column) on MgO(100) (top row), $SrTiO_3(100)$ (middle row), and $LaAlO_3(100)$ (bottom row). The ranges for the height contrast for the AFM images of 5, 10, and 50 min films are 30, 30, and 60 nm, respectively.

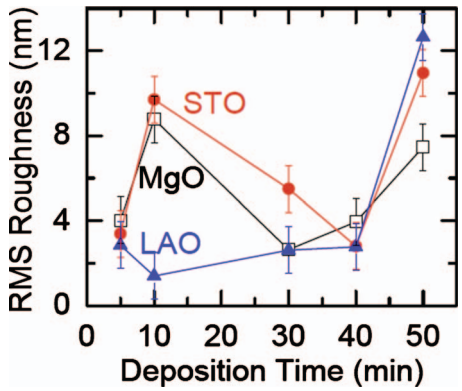

FIG. 3. rms roughness as a function of deposition time for Sr_2MoFeO_6 films grown on MgO(100), $SrTiO_3(100)$, and $LaAlO_3(100)$. The rms roughness is obtained over a 12 μm^2 scanned area of the respective AFM image.

the (004) peak by registering the presence of the high intensity (112) peak in a position consistent with a c-axis aligned film. Phi scans about the SFMO(112) reflection show the expected fourfold symmetry and no indication of any other in-plane rotational variants.

Figure 2 shows the AFM images of the SFMO films grown on MgO, STO, and LAO for selected deposition times of 5, 10, and 50 min. Based on our previous analysis,[25] the rate of deposition was estimated to be 4 ± 2 nm/min. Although the films were all grown simultaneously under the same growth conditions, there are clear differences among the morphologies of the films on the three substrates. The AFM image of the SFMO on MgO [Fig. 2(a)] shows a large number of square terraces with an epitaxial relationship to one another and presumably with the MgO substrate. After 10 min of growth [Fig. 2(b)], the SFMO terraces have become larger, and growth spirals are visible. At a longer deposition time [Fig. 2(c)], the surface looks smooth but with cuboid nanoparticles (with ~90 nm side lengths) atop the film. Given that the XRD measurement for this film does not reveal any peaks other than SFMO (002) and (004), it is likely that the volume of these nanoparticles is not sufficiently large to be detectable by XRD. Further analysis is required to determine the nature of these nanoparticles. For the SFMO film growth on STO, the 5 min film appears to have layered structures with larger square terraces [Fig. 2(d)], which have evidently become layers in the 10 min film and the resulting surface appears smooth [Fig. 2(e)]. Similar layer morphology has been reported by Manako *et al.*[13] The elevated square features in Figs. 2(d) and 2(e) have also been observed by other groups.[12,26] The resulting film on STO after 50 min of deposition remains smooth with a few nanoparticles, with ~70 nm side lengths [Fig. 2(f)], as was similarly observed for MgO [Fig. 2(c)]. Figure 2(g) shows flake-like nanostructures for the 5 min SFMO film grown on LAO, which become larger in the 10 min film [Fig. 2(h)]. The surfaces of the films on LAO appear to be the least ordered relative to the corresponding films grown on MgO and STO, with the largest density of nucleation sites and few obvious terraces or growth spirals. The 50 min SFMO film grown on LAO appears smooth [Fig. 2(i)], with a discernibly larger density of cuboid nanoparticles (with ~100 nm side lengths) than films grown on MgO and STO. The differences in morphology among the SFMO films grown on the three substrates are most obvious for the thinner films, and the appearances of the films become similar with increasing deposition time. The presence of nanoparticles, less than 100 nm in diameter, on the 50 min films grown on all three substrates suggests that these nanoparticles could originate from the same particulate formation mechanism possibly due to changes in the surface condition of the SFMO target after extended ablation. The larger particles (~350 nm in size), also observed in the 50 min films, may be due to formation of secondary phases such as Fe_2O_3, MoO_2, and $SrMoO_4$ or a-axis aligned SFMO grains, to be discussed below.

The AFM data indicate that SFMO grows differently on different substrates. The SFMO films deposited on STO [Figs. 2(d)–2(f)] and, to a lesser extent, on MgO [Figs. 2(a)–2(c)] tend to grow more two dimensionally as in Frank–van der Merve or Stranski–Krastanov growth, while the films on LAO [Figs. 2(g)–2(i)] tend to show Volmer–Weber growth, where there is isolated island growth in three dimensions.[27]

The root-mean-square (rms) roughness determined over the 12 μm^2 scanned area of the respective AFM images of the films grown on the three substrates is plotted as a function of deposition time in Fig. 3. The estimated error bars of ± 1.1 nm were obtained by the standard deviation of five different measurements at different sampling points on one of the 50 min films. Although all the films deposited on MgO, STO, and LAO have similar rms roughness of 3–4 nm after 5 min of growth, SFMO films grown on MgO and STO show greatly increased roughness after 10 min of growth. The increased rms roughness for the SFMO films after the 10 min growth on the MgO and STO substrates is consistent with the larger terraces and growth spirals observed in Figs. 2(b) and 2(e). As the growth of these films continues to 40 min of deposition, the reduction in their RMS roughness parameters is in accord with the layer-by-layer growth mode. On the other hand, the SFMO films grown on LAO have a relatively constant roughness up to 40 min of growth, which is consistent with the Volmer–Weber growth mode observed

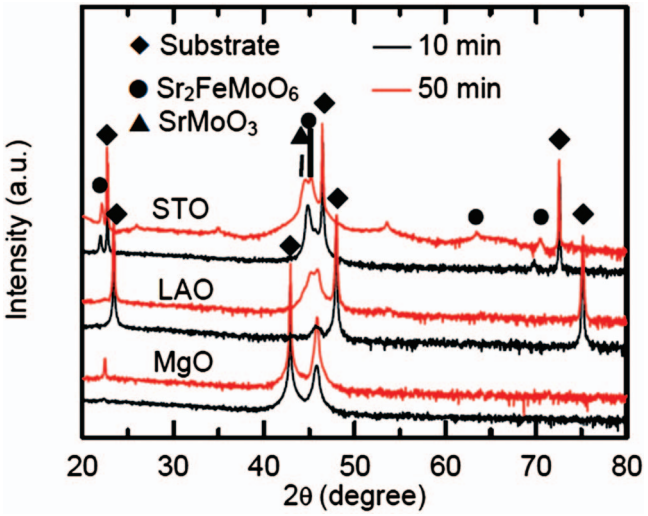

FIG. 4. (ω-2θ) scans (in logarithmic intensity scale) of Sr_2FeMoO_6 films PLD-grown on MgO(100) (bottom), $LaAlO_3$(100) (middle), and $SrTiO_3$(100) (top) in vacuum with a laser fluence of 400 mJ/pulse at 800 °C for 10 min (darker/lower lines) and 50 min (lighter/upper lines). Features corresponding to Sr_2FeMoO_6 (Ref. 21), $SrMoO_3$ (Ref. 28), and the substrates $SrTiO_3$, $LaAlO_3$, and MgO are identified by solid circles (●), solid triangles (▲), and solid diamonds (◆), respectively. The curves have been offset by a multiplicative constant for clarity.

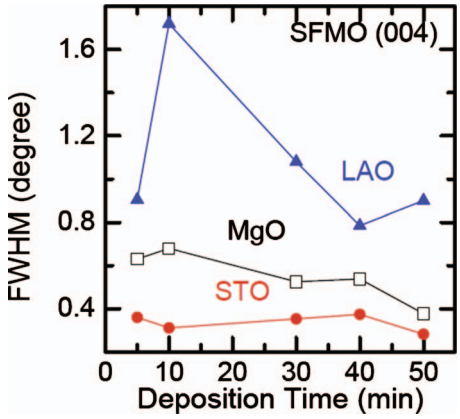

FIG. 5. FWHM of the SFMO(004) peak in the rocking curve measurement as a function of deposition time for Sr_2FeMoO_6 films grown on MgO(100), $SrTiO_3$(100), and $LaAlO_3$(100).

in Fig. 2. The sudden increase in the rms roughness for the SFMO films grown on all three substrates after 50 min of deposition can be attributed to particulate formation as noted above. The layer-by-layer growth seen in the SFMO film on STO is expected due to the low strain caused by the small lattice mismatch (−1.2%) between STO and SFMO. However, layer-by-layer growth is also found for the SFMO film on MgO, where the lattice mismatch is considerably larger (+6.2%). This is surprising especially when Volmer–Weber growth is observed for SFMO film growth on LAO, where the lattice mismatch (−4.3%) is smaller.

To further investigate the crystal quality of the SFMO films grown on the three substrates, detailed x-ray diffraction studies were carried out. Figure 4 shows the ω-2θ scans for selected SFMO films deposited for 10 and 50 min on MgO(100), LAO(100), and STO(100). In addition to the substrate peaks, two prominent SFMO planes of (002) (at 2θ =22.5°) and (004) (at 2θ=45.8°) can be observed, which indicate that the SFMO films were all epitaxially grown along the c-axis of the substrates. For the films grown on MgO, no other features can be seen regardless of the deposition time. However, for the films deposited on STO and LAO, even though thinner films (with deposition time less than 20 min) are single-phase, increasing the deposition time promotes the growth of an additional $SrMoO_3$ phase (Ref. 28).[26] These $SrMoO_3$ peaks are indicative of epitaxial material, and reflect regions of antisite disorder (Fe/Mo) in the SFMO film. However, no x-ray diffraction peaks were observed for the corresponding $SrFeO_3$ phase. The thick film grown on STO also showed the presence of some very small peaks that may be attributed to Fe and Mo oxides. This result is in marked contrast to the work by Boucher,[18] who grew SFMO films with different thicknesses on several substrates by magnetron sputtering and noted small parasitic phases for all his films, primarily $SrMoO_3$ in films grown on MgO, SrO in films grown on STO, and FeO and $SrMoO_4$ in films grown on LAO.

Rocking curve analysis has been performed to extract the widths of the (004) diffraction peak of SFMO films grown on the three substrates for different deposition times, shown in Fig. 5. The XRD configuration is the same as that used in the Bragg scans, except for the removal of the 1/16° defining slit for the diffracted beam. STO has the least lattice mismatch with SFMO and has the lowest value for the full width at half maximum (FWHM) of the rocking curve (0.34°). There is virtually no change in the FWHM for longer deposition times, indicating consistent crystalline quality even for thicker films. For the SFMO films grown on MgO (with a positive lattice mismatch of greater magnitude than STO), the corresponding rocking curve has a larger FWHM value of 0.63° for the 5 min deposition and then decreases slowly to 0.37° for 50 min deposition, indicating a decrease in mosaic spread for the thicker films. Consistent with the AFM images presented in Fig. 2, the SFMO films on LAO (with a larger negative lattice mismatch than STO) exhibit the largest FWHM values between 0.9° and 1.7°, and the FWHM value appears to decrease with increasing deposition time.

In order to study the evolution of the crystal quality during epitaxial growth, reciprocal space map measurements were performed to extract in-plane and out-of-plane lattice parameters for all the samples. In RSM, the lattice mismatch and degree of relaxation are independent of the ω and 2θ scanning ratio and the miscut of the surface with respect to the diffraction lattice plane. By using the Ge(220) analyzer in the triple-axis section to condition the diffracted beam, it is possible to achieve high enough resolution to resolve close-lying features.[29] A series of ω-2θ scans around the symmetric SFMO(004) plane (ω=22.9°, 2θ=45.80°, ϕ=0°, and ψ =0°) and asymmetric SFMO(112) plane (ω=15.97°, 2θ =31.94°, ϕ=0°, and ψ=45°) was performed to construct the RSMs. Commercial software, PANALYTICAL EXPERT EPITAXY, was used to analyze the data.[30,31] Different color contrast indicates different intensities on a log scale, and because the step sizes and dwell times were not the same for the scans in

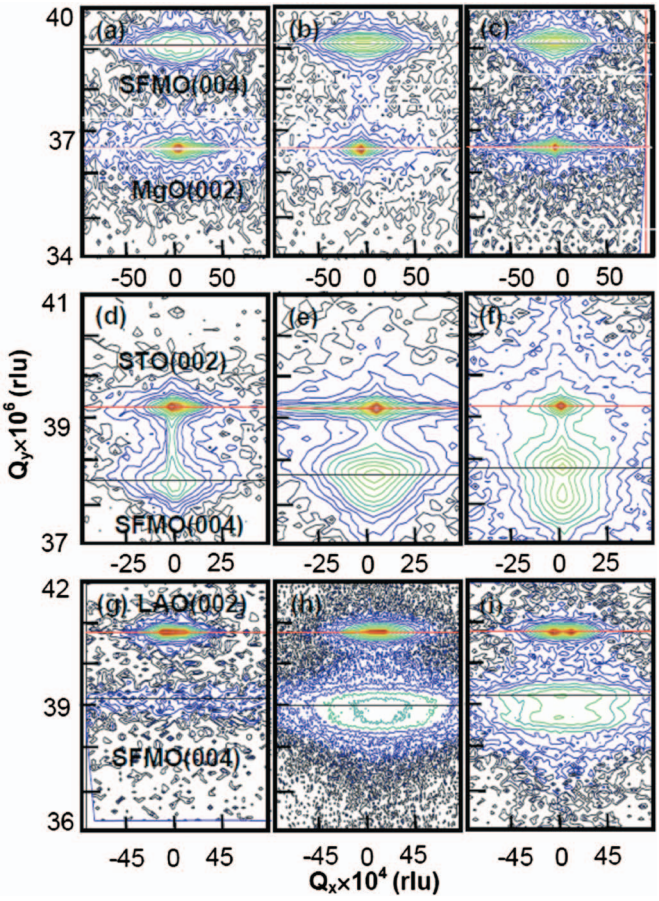

FIG. 6. Reciprocal space maps (in reciprocal length unit or RLU) of the (004) plane of Sr_2FeMoO_6 films grown on the (100) plane of MgO (top row), $SrTiO_3$ (middle row), and $LaAlO_3$ (bottom row) for 5 min (left column), 30 min (center column), and 50 min (right column).

all the measurements, the intensities from map to map are not comparable.

Figure 6 shows the RSMs for the SFMO (004) plane, each of which depicts an intense (002) substrate peak and a considerably weaker and broader (004) SFMO peak. The substrate peak position in Q_y is indicated by a red dashed line, while the SFMO peak position is marked by the black solid line. For SFMO on MgO (Fig. 6, top row), there is little change in either the shape or position of the SFMO(004) peak with deposition time. While the MgO lattice mismatch with SFMO should put the film under tensile strain (with a +6.2% lattice mismatch), there is negligible change in the c-axis parameter in the as-grown SFMO film when compared to bulk SFMO, and no evidence of strain relaxation is found in even the thickest films. On the other hand, the negative lattice mismatches between the STO (−1.2%) and LAO substrates (−4.1%) with the SFMO films should induce compressive strain in the SFMO films. The characteristic twinning of the LAO substrate is characterized by the splitting of the LAO (002) peak along the Q_x direction. For both these substrates, the SFMO peak is moving along the positive Q_y direction with increasing deposition time. As will be seen explicitly in Fig. 8, this peak shift reflects that the c-axis lattice length of the SFMO film on STO and LAO is approaching that of the bulk SFMO and is indicative of strain

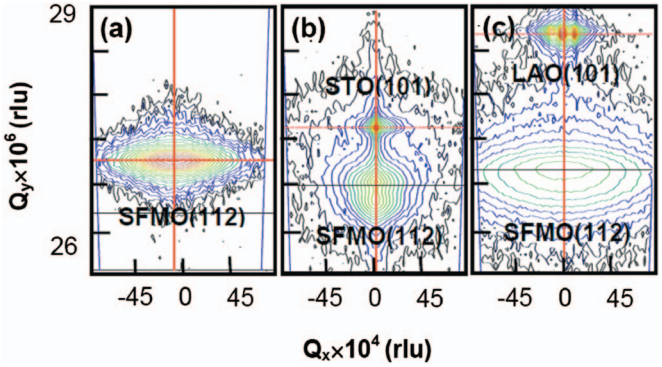

FIG. 7. Reciprocal space maps (in RLU) of the (112) plane of Sr_2FeMoO_6 films PLD-grown on the (100) plane of MgO (right), $SrTiO_3$ (center), and $LaAlO_3$ (left) for 50 min.

relaxation. Another indicator of a film undergoing strain relaxation is the triangular shape of the film diffraction peak. For the STO (Fig. 6, middle row) and LAO substrates (Fig. 6, bottom row), it is not possible to determine if this triangular peak shape occurs due to the emergence of a second peak near the broad SFMO peak along the Q_y direction. This second peak can be assigned to $SrMoO_3$(002) and is also observed in the corresponding ω-2θ scans for STO and LAO in Fig. 4. The creation of this secondary phase appears to release the strain, allowing the SFMO film lattice parameters to more closely approach those of bulk SFMO.

In order to further investigate the origin of the weak secondary film peak observed in Fig. 6, we show in Fig. 7 the corresponding RSMs for the SFMO(112) plane for the 50 min films grown on the three substrates. Evidently, the SFMO peak for the MgO substrate [Fig. 7(a)] is symmetrical and well defined and is found to exhibit a narrow FWHM in the Q_y direction. There is some broadening in the Q_x direction, indicating the presence of a significant number of lattice defects, such as misfit dislocations and subgrain boundaries. No substrate peak is visible due to the high symmetry of the MgO structure. For the STO substrate [Fig. 7(b)], both the strong STO(101) and the weaker SFMO(112) peaks can be seen. The SFMO peak is clearly bimodal in the Q_y direction, consistent with the presence of two phases. There is relatively less broadening in the Q_x direction, in accord with a smaller number of lattice defects. For the LAO substrate [Fig. 7(c)], we can also observe both the intense LAO(101) and weaker SFMO(112) peaks. The LAO substrate peak has split into a number of peaks in the Q_x direction, indicative of twinning. The SFMO(112) forms a single broad peak, with large FWHMs in both the Q_x and Q_y directions, and it appears to be asymmetric in the Q_y direction. While there may be a secondary phase formation in the SFMO on LAO film, the off-axis peak is obscured by the broadening due to poor substrate quality and lattice defects in the film.

The behavior of lattice parameters of the SFMO film during growth on the three substrates can be quantified by examining the changes in the a-, b-, and c-axis lengths as a function of deposition time, as shown in Fig. 8. From the RSM depicted in Fig. 6, the c-axis length can be determined from the separation of the film and substrate peak positions.[30] From the RSM of the SFMO(112) plane (Fig. 7)

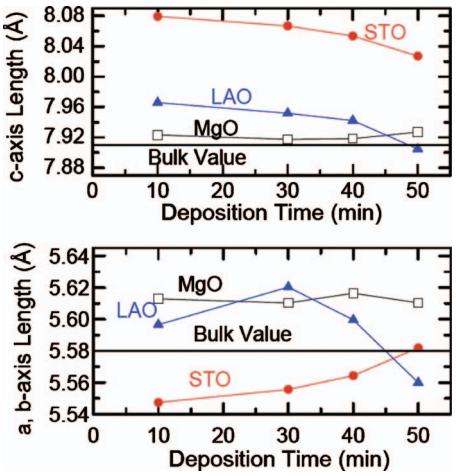

FIG. 8. c-axis length (top) and a- and b-axis lengths (bottom) as a function of deposition time for Sr_2FeMoO_6 films grown on MgO(100), $SrTiO_3$(100), and $LaAlO_3$(100).

and the c-axis length determined from Fig. 6, we obtain the corresponding a and b axis lengths. For the STO substrate, with its small lattice mismatch (−1.2%), the c-axis lengths of the SFMO films are found to be the largest, in agreement with earlier work.[14,15,18] This c-axis enlargement is consistent with a strained film. Furthermore, the decrease in the c-axis length toward the bulk value obtained for SFMO powder, 7.918 Å [(Ref. 21)], with increasing deposition time can be viewed as due to strain relief in a thicker film. Consistent with a strain effect, the a- and b-axis lengths are smaller than the respective bulk values in the thinnest films, and they reach the bulk values (5.58 Å) for the 50 min films. For the SFMO films grown on LAO (with a lattice mismatch of −4.3%), the c-axis length also follows a decreasing trend with increasing deposition time from 10 to 50 min of deposition, similar to that found for the SFMO films on STO. Unlike STO, the corresponding a- and b-axis lengths are also larger than the respective bulk values and approach the bulk values for the longer deposition times. This may indicate oxygen deficiency in the SFMO on LAO films, excessive Fe/Mo disorder, or perhaps some doping of the film by the substrate. Although Boucher[18] did not determine the a- and b-axis lengths, he did find that the c-axis lengths for the SFMO films on LAO are smaller than those for SFMO films on STO. Interestingly, the a-, b-, and c-axis lengths for the SFMO films on MgO (with a lattice mismatch of +6.2%) are found to be the closest to the bulk value, and they appear almost constant and independent of the film thickness.

Using the lattice parameters, the unit cell volumes of the SFMO films have been calculated. For the SFMO grown on STO, the volume increases from 248.6 $Å^3$ (for the 10 min film) to 250.1 $Å^3$ (for the 50 min film), while the corresponding volume for the SFMO films grown on MgO was almost constant (249.4 ± 0.3 $Å^3$). The unit cell volume values obtained for all the SFMO films grown on different substrates are all larger than the bulk value of 246 $Å^3$.

For all the SFMO films, the c-axis length is larger than the bulk value. This large out-of-plane c-axis length for SFMO films has also been noted by several other groups.[12,14,32] The observed larger c-axis value has been attributed to several origins, including a change in the ordering of the Fe and Mo atoms in the lattice,[14,26,33] thermal strain induced by different thermal expansion coefficients upon cooling from the growth temperature,[32] lattice mismatch (for SFMO films grown on STO),[14] structural film defects,[12] and off-stoichiometry of the cations.[18] For example, Sanchez *et al.*[12] reported the variation of c-axis length for SFMO on STO as a function of deposition temperature, deposition rate, and film thickness. Their results showed that the c-axis length decreases toward the bulk value with increasing growth temperature and decreasing deposition rate.

For SFMO films on LAO, because its negative lattice mismatch (−4.3%) is much larger in magnitude than that on STO (−1.2%), one might expect these films to also have larger c-axis lengths than those on STO. On the other hand, the SFMO films on LAO are found to have more nucleation sites and more defects than those on STO, as seen from the rocking curve data in Fig. 5. The presence of these defects in the former films may relieve the strain caused by the lattice mismatch and allow the c-axis lengths to relax to a value closer to that of bulk SFMO. For the SFMO films grown on MgO, the tensile strain (as a result of a positive lattice mismatch of +6.2%) would lead a strained SFMO c-axis length to be less than the bulk value, in contrast to that observed in Fig. 8. Furthermore, the c-axis length is found to be relatively constant with increasing film thickness. Boucher also observed the near-independence of the c-axis length with thickness for SFMO films deposited on MgO by magnetron sputtering.[18] He attributed this result to reorganization of the SFMO films on MgO, similar to what was seen in $La_{0.7}Sr_{1.3}MnO_3$ on MgO by Gommert *et al.*[34] In $La_{0.7}Sr_{1.3}MnO_3$, the mismatch strain with MgO was found to be completely compensated in a narrow interface region of the substrate, after which the film grows with few defects and little strain.

The observation from Fig. 7, that the SFMO unit cell volume is increased for all the films from that of the bulk, would tend to support the hypothesis that the changes in c-axis length are due to more than just lattice mismatch (strain) effects and the film quality of epitaxially grown films is strongly influenced by additional factors such as Fe/Mo ordering, oxygen concentration, lattice defects (vacancies and interstitials), and substrate-film interdiffusion.

IV. CONCLUSIONS

Using pulsed laser deposition, we have grown near-epitaxial SFMO films on three different substrates with different lattice matches: MgO(100) (+6.2%), STO(100) (−1.2%), and LAO(100) (−4.3%). In order to study the effects of strain induced by substrates on the growth evolution of the SFMO films, we have deposited films on all three substrates simultaneously (under the same growth conditions) for different deposition times, corresponding to different film thicknesses of 20–200 nm. Using AFM, we observed different evolutions of surface morphology with increasing film thickness on the three substrates. In particular, SFMO grown on LAO has the highest number of nucleation sites, and three-dimensional growth can be clearly observed from

the early stage. For SFMO grown on MgO and STO, even though MgO contains more nucleation sites than STO, the observed growth trends were similar to each other. For both of these substrates, the SFMO films tend to grow layer by layer in the early stage, with a large number of square terraces forming an epitaxial relationship with the substrate. This initial layer-by-layer growth is followed by spiral growth clusters and three-dimensional growth at longer deposition times.

We also performed high-resolution XRD and RSM measurements, which indicate that there is epitaxial growth of Sr_2FeMoO_6 films on all three substrates. Rocking curve analysis shows that the SFMO films on STO and LAO have the smallest and largest FWHMs, respectively. Although SFMO and MgO have the largest lattice mismatch, the FWHM of the SFMO film on MgO lies between the STO and LAO values, suggesting a different growth mechanism for the positive lattice mismatch seen with the MgO substrate. While the lattice parameters (a-, b-, and c-axis lengths) of the as-grown SFMO films on STO and LAO are found to converge to the bulk value, reflecting reduced strain in the thicker SFMO films, the lattice parameters for SFMO on MgO remain relatively constant. For all the films, the cell volume is greater than that determined for bulk SFMO. For films with thickness greater than ~120 nm, Bragg diffraction scans and RSM revealed secondary phase formation on the STO and LAO. The Bragg XRD measurements showed that a higher deposition time promotes the formation of an epitaxial parasitic phase (i.e., $SrMoO_3$) on STO and LAO but not on those grown on MgO substrates. The formation of $SrMoO_3$ is indicative of a significant level of antisite disorder and may provide strain relief from the negative lattice mismatch of SFMO films grown on STO and LAO. The present work shows that MgO, despite its large lattice mismatch, appears to be fully relaxed at the early growth stage, therefore offering the best substrate for growing high quality, epitaxial, single-phase SFMO films.

ACKNOWLEDGMENTS

This work was supported by the Natural Sciences and Engineering Research Council of Canada. We thank S. Bazargan, Dr. S. Speakman, and Dr. I. Cernatescu for their technical assistance and helpful discussions.

[1] F. S. Galasso, *Structure, Properties and Preparation of Perovskite-Type Compounds* (Pergamon, London, 1969).
[2] K.-I. Kobayashi, T. Kimura, H. Sawada, K. Terakura, and Y. Tokura, Nature (London) **395**, 357 (1998).
[3] M. Bibes, K. Bouzehouane, A. Barthelemy, M. Besse, S. Fusil, M. Bowen, P. Seneor, J. Carrey, V. Cros, A. Vaures, J.-P. Contour, and A. Fert, Appl. Phys. Lett. **83**, 2629 (2003).
[4] J. Navarro, L. I. Balcells, F. Sandiumenge, M. Bibes, A. Roig, B. Martinez, and J. Fontcuberta, J. Phys.: Condens. Matter **13**, 8481 (2001).
[5] M. García-Hernández, J. L. Martinez, M. J. Martinez-Lope, M. T. Casais, and J. A. Alonso, Phys. Rev. Lett. **86**, 2443 (2001).
[6] Q. Gan, R. A. Rao, C. B. Eom, J. L. Garrett, and M. Lee, Appl. Phys. Lett. **72**, 978 (1998).
[7] C. U. Jung, H. Yamada, M. Kawasaki, and Y. Tokura, Appl. Phys. Lett. **84**, 2590 (2004).
[8] U. Gebhardt, N. V. Kasper, A. Vigliante, P. Wochner, H. Dosch, F. S. Razavi, and H.-U. Habermeier, Phys. Rev. Lett. **98**, 096101 (2007).
[9] R. B. Praus, G. M. Gross, F. S. Razavi, and H.-U. Habermeier, J. Magn. Magn. Mater. **211**, 41 (2000).
[10] F. S. Razavi, G. V. Sudhakar Rao, H. Jalili, and H.-U. Habermeier, Appl. Phys. Lett. **88**, 174103 (2006).
[11] M. Besse, F. Pailloux, A. Barthelemy, K. Bouzehouane, A. Fert, J. Olivier, O. Durand, F. Wyczisk, R. Bisaro, and J.-P. Contour, J. Cryst. Growth **241**, 448 (2002).
[12] D. Sánchez, M. García-Hernández, N. Auth, and G. Jacob, J. Appl. Phys. **96**, 2736 (2004).
[13] T. Manako, M. Izumi, Y. Konishi, K.-I. Kobayashi, M. Kawasaki, and Y. Tokura, Appl. Phys. Lett. **74**, 2215 (1999).
[14] W. Westerburg, D. Reisinger, and G. Jakob, Phys. Rev. B **62**, R767 (2000).
[15] S. R. Shinde, S. B. Ogale, R. L. Greene, T. Venkatesan, K. Tsoi, S.-W. Cheong, and A. J. Millis, J. Appl. Phys. **93**, 1605 (2003).
[16] R. P. Borges, S. Lhostis, M. A. Bari, J. J. Versluijs, J. G. Lunney, J. M. D. Coey, M. Besse, and J.-P. Contour, Thin Solid Films **429**, 5 (2003).
[17] H. Q. Yin, J.-S. Zhou, J.-P. Zhou, R. Dass, J. T. McDevitt, and J. B. Goodenough, Appl. Phys. Lett. **75**, 2812 (1999).
[18] R. Boucher, J. Phys. Chem. Solids **66**, 1020 (2005).
[19] H. Asano, M. Osugi, Y. Kohara, D. Higashida, and M. Matsui, Jpn. J. Appl. Phys., Part 1 **40**, 4883 (2001).
[20] H. Jalili, N. F. Heinig, and K. T. Leung, Phys. Rev. B **79**, 174427 (2009).
[21] JCPDS 01-070-4092.
[22] JCPDS 00-045-0946.
[23] JCPDS 00-035-0734.
[24] JCPDS 01-085-0848.
[25] H. Jalili, N. F. Heinig, and K. T. Leung, J. Appl. Phys. **105**, 034305 (2009).
[26] A. Venimadhav, M. E. Vickers, and M. G. Blamire, Solid State Commun. **130**, 631 (2004); A. Venimadhav, F. Sher, J. P. Attfield, and M. G. Blamire, J. Magn. Magn. Mater. **269**, 101 (2004).
[27] J. Venable, *Introduction to Surface and Thin Film Processes* (Cambridge University Press, Cambridge, UK, 2000).
[28] JCPDS 00-024-1224.
[29] V. Holy, U. Pietsch, and T. Baumbach, *High-Resolution X-Ray Scattering from Thin Films and Multilayers* (Springer-Verlag, Berlin, 1999).
[30] PANALYTICAL EXPERT EPITAXY SOFTWARE, X'Pert MRD application.
[31] M. Birkholz, *Thin Film Analysis by X-Ray Scattering* (Wiley-VCH Verlag, Weinheim, 2006).
[32] T. Fix, D. Stoeffler, S. Colis, C. Ulhaq, G. Versini, J. P. Vola, F. Huber, and A. Dinia, J. Appl. Phys. **98**, 023712 (2005).
[33] H. Asano, S. B. Ogale, J. Garrison, A. Orozco, Y. H. Li, E. Li, V. Smolyaninova, C. Galley, M. Downes, M. Rajeswari, R. Ramesh, and T. Venkatesan, Appl. Phys. Lett. **74**, 3696 (1999).
[34] E. Gommert, H. Cerva, J. Wecker, and K. Samwer, J. Appl. Phys. **85**, 5417 (1999).